HHS Public Access

Author manuscript

Adv Healthc Mater. Author manuscript; available in PMC 2023 July 01.

Published in final edited form as:

Adv Healthc Mater. 2022 July ; 11(13): e2200170. doi:10.1002/adhm.202200170.

Soft Wireless Bioelectronics Designed for Real-Time, Continuous Health Monitoring of Farmworkers

Yun-Soung Kim[1], **Jihoon Kim**[1], **Roxana Chicas**[2], **Nezahualcoyotl Xiuhtecutli**[3,4], **Jared Matthews**[1], **Nathan Zavanelli**[1], **Shinjae Kwon**[1], **Sung Hoon Lee**[1], **Vicki S. Hertzberg**[2], **Woon-Hong Yeo**[1,2,5,6,7,8]

[1]George W. Woodruff School of Mechanical Engineering and IEN Center for Human-Centric Interfaces and Engineering, Georgia Institute of Technology, Atlanta, GA, 30332, USA.

[2]Parker H. Petit Institute for Bioengineering and Biosciences, Georgia Institute of Technology, Atlanta, GA, 30332, USA.

[3]Farmworker Association of Florida, Apopka, FL, 32703, USA.

[4]Department of Anthropology, Tulane University, New Orleans, LA, 70118, USA.

[5]Wallace H. Coulter Department of Biomedical Engineering, Georgia Tech and Emory University, Atlanta, GA, 30332, USA.

[6]Institute for Materials, Georgia Institute of Technology, Atlanta, GA, 30332, USA.

[7]Neural Engineering Center, Georgia Institute of Technology, Atlanta, GA, 30332, USA.

[8]Institute for Robotics and Intelligent Machines, Georgia Institute of Technology, Atlanta, GA, 30332, USA.

Abstract

Hotter summers caused by global warming and increased workload and duration are endangering the health of farmworkers, a high-risk population for heat-related illness (HRI) and deaths. Although prior studies using wearable sensors show the feasibility of employing field-collected data for HRI monitoring, existing devices still have limitations, such as data loss from motion artifacts, device discomfort from rigid electronics, difficulties with administering ingestible sensors, and low temporal resolution. Here, this paper introduces a wireless, wearable bioelectronic system with functionalities for continuous monitoring of skin temperature, electrocardiograms (ECG), heart rates (HR), and activities, configured in a single integrated package. Advanced nanomanufacturing based on laser machining allows rapid device fabrication and direct incorporation of sensors with a highly breathable substrate, allowing for managing

*Corresponding author: whyeo@gatech.edu.

Author Contributions

Y.-S.K. and J.K. contributed equally to this work. W.-H.Y. and V.H. conceived and designed the research; Y.-S.K., J.K., and S.K. fabricated the device; Y.-S.K., J.K., R.C., and N.X. performed the experiment; Y.-S.K., J.K., J.M., N.Z., and S.H.L. analyzed the data; N.X. recruited the study participants; Y.-S.K. and W.-H.Y. wrote the paper.

Supporting Information

Supporting Information is available from the Wiley Online Library or from the author.

Conflict of Interest

Georgia Tech has a pending US patent application.

excessive sweating and multi-modal stresses. To validate the device's performance in agricultural settings, we apply the device to multiple farmworkers at various operations, including fernery, nursery, and crop. The accurate data recording, including high-fidelity ECG (signal-to-noise ratio: > 20 dB), accurate HR ($r = 0.89$, $r^2 = 0.65$ in linear correlation), and reliable temperature/activity, confirms the device's capability for multi-parameter health monitoring of farmworkers.

Graphical Abstract

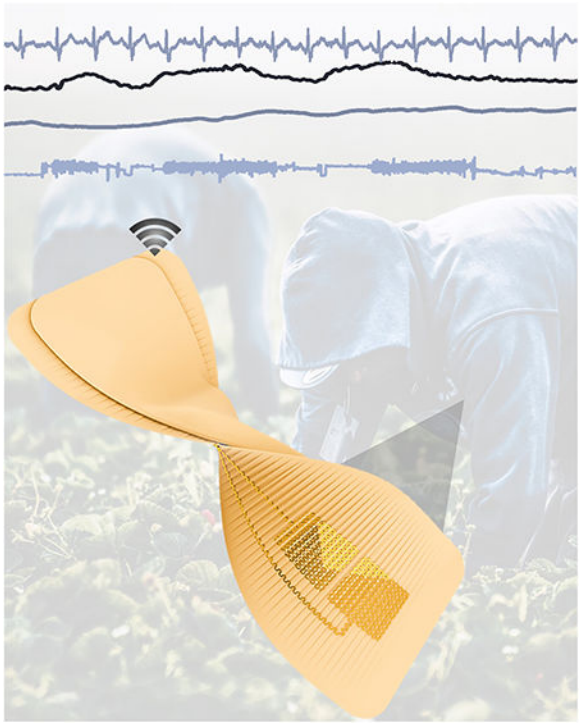

This image shows a soft wearable electronic patch designed for real-time, continuous health monitoring of farmworkers by measuring skin temperature, electrocardiograms, heart rates, and activities.

Keywords

health monitoring of farmworkers; soft electronics; wireless systems; micromachining; heat-related illnesses

1. Introduction

Agricultural workers have been identified as a vulnerable occupational group with an increased risk of adverse health outcomes caused by exposure to a combination of elevated temperature, humidity, solar radiation, and physical activities.[1] A survey conducted by the Centers for Disease Control and Prevention between 1992 and 2006 reports a total of 423 heat-related deaths in agricultural and nonagricultural settings, where most of the deceased were agricultural workers between the ages 20 and 54.[2] An analysis of the US census

for fatal occupational injuries shows that heat-related mortality in agricultural workers is 35 times greater than the general workforce population.[3] Though less severe than death, consequences for working in hot environments include increased likelihood of experiencing occupational HRI and negative effects on health and productivity.[4] As part of the trend in global climate change, the warmest temperature of each summer is surpassing prior records, while more regions in North America and Europe are expected to suffer from severe heat waves during the next century.[5] Unfortunately, the occupational setting for agricultural workers does not aid in response to such extreme weather but demands physically strenuous physical outdoor activities for farmworkers, who often have little control over their heat exposure, and a greater risk of HRI from extreme heat is expected for this population. Efforts to provide heat-related guidance for agricultural workers have been made, such as the recommendations set forth by the National Institute for Occupational Safety and Health and the Occupational Safety and Health Administration, and the National Fire Protection Association, along with an increasing number of consensus publications including the recent publications by Morrissey et al.[6–11] In the US, however, there is no federal standard to protect workers from excessive heat exposure, and only three states, California, Minnesota, and Washington, have implemented such mandates.

One of the main causes for worker protection against heat stress is the lack of real-world data detailing the physiologic assessments in actual high-heat agricultural settings. To date, an effort that directly examines physiologic responses to hard labor in hot agricultural environments is limited to field studies conducted by researchers, who deployed wearable devices to record the health of farmworkers in Central Florida between 2012 and 2017.[12–14] Though it was concluded that real-world physiologic health monitoring of farmworkers is possible, the studies revealed several limitations. The set of wearable devices used, including the HR chest strap (Polar T31, Polar Electro) and the waist-worn accelerometer (ActiGraph GTX3+, ActiGraph), are inherently uncomfortable to wear and obstructive to participants' motion, especially during tasks requiring repeated movements. In addition, administration of the ingestible pill (CorTemp Ingestible Core Body Temperature Sensor, HQInc.) for core body temperature (T_c) measurement needs to be conducted carefully to ensure the passage time covers the duration of workday. The pill sensor, resembling a large vitamin pill, also creates unique challenges in participation uptake due to its size (2.2 cm long, 1.1 cm diameter) and tendency for the spread of misinformation within a community. Finally, successful collection of both HR and T_c requires that the strap and pill sensors maintain a close distance (a radial range of 60 cm) to a bulky receiver (CorTemp Data Recorder) worn around a participant's waist. Similar challenges associated with complicated device setup and bulkiness of individual sensors are anticipated for recent studies on occupational health monitoring that rely on rigid sensor modules affixed to the body with straps and belts. Recently, several demonstrations showing soft wearable sensors implemented in the areas of disease diagnosis, remote health monitoring, and human performance enhancement, mainly through the means of human-machine interfaces, the effort to apply the technological advances toward ensuring the safety of outdoor workers has been missing.[15–17] A soft device developed by Jeong et al. in 2021 is the closest representation of the utility of soft wearable sensors implemented in an occupational setting. However, the study does not include field validation of the device in real-life occupational

settings but focuses on its multifunctional characteristics.[18] Consequently, there is an immediate need for a health monitoring scheme that does not interfere with worker motions and is robust in hot, humid, high-motion settings, able to continuously monitor parameters relevant for physiological responses to heat and work intensity, and imperceptible to both users and observers to avoid unnecessary attention.

Here, this work introduces an engineering solution as a response to the need for better health monitoring of agricultural workers. The bioelectronic sensor system is designed to be attached to the user's chest for multi-parameter monitoring, namely skin temperature, ECG, HR, and activity, and is referred to as biopatch here on. The self-adhesiveness of the biopatch allows the device to remain adhered to the chest without requiring additional contraptions, while its compact form factor allows minimal interference with worker motion. Assembled on a highly breathable medical adhesive, the biopatch can efficiently pass sweat and body fluids to ensure robust adhesion despite mechanically and environmentally demanding settings. The flexible wireless sensor module is sealed with an elastomer to guarantee reliable operation under extreme environmental stresses, including exposure to elevated temperature, humidity, contacts with clothing and particles from crops. The feasibility of using the biopatch for field-based physiologic data collection in agricultural settings is verified by deploying the devices in two groups of farmworkers recruited in Apopka and Pierson, Florida, in July 2021. The set of results presented here suggests the biopatch's potential role as an accurate, convenient, and robust occupational health monitoring platform in agricultural sectors and beyond.

2. Results and Discussion

2.1. Overview of biopatch design, functionality, and data processing

Configured in a light (6.5 g), compact footprint (8.5 cm × 4.0 cm), and thin flexible (0.28 mm for the adhesive, 3.0 mm for the module) profile, a fully packaged biopatch can be easily handled by general users without requiring additional tools or specific training. The wireless sensor module containing a rechargeable lithium-ion polymer battery (105 mA, LP401230, Adafruit), integrated circuit (IC) components necessary for sensing, signal processing, and wireless communication based on Bluetooth Low Energy (BLE) is packaged in a $3 \times 3 \times 0.3$ cm^3 compliant and rugged module, with a magnetic port for battery charging and a slide switch to power on and off the device (Figure 1A). As shown in Figure 1B, the breathable adhesive tape (9907T, 3M™) affixes the module to the skin and serves as the adhesive for the thin-film ECG electrodes integrated directly into the adhesive side. For additional protection, the wireless module against rain, particles from crops, and rubbing of user's clothes, a smaller tape is applied over the module as a cover tape (Figure 1C). This study follows the device placement guideline described in our previous report, in which the bipolar electrodes are intended to mimic precordial (transverse plane) lead V2 of a conventional 12-lead setup.[19] As shown in Figure 1D, the biopatch is positioned vertically along the centerline of the chest, below the suprasternal notch to minimize motion-induced artifacts with the positive and negative electrodes toward the feet and head, respectively. Once attached to the chest and powered on, the biopatch can establish a BLE connection with an Android smartphone, which can be carried in the user's pocket or in a fanny

pack and continuously transmit ECG, skin temperature, and accelerometer data for up to 12 hours, a duration sufficient to cover a typical workday. A diagram shown in Figure 1E illustrates the overall aim of the biopatch development and its implementation in an agricultural environment. The biopatch's key design considerations include the ability to operate in elevated levels of heat, temperature, sweat, and motion, to enable continuous monitoring of ECG, HR, skin temperature, and activity. Specifically, time-varying skin surface potential is captured by the stretchable bipolar electrodes at 250 Hz and is passed to a front-end analog-to-digital converter (ADC, ADS1292, Texas Instruments). A high-precision digital temperature sensor (TMP117, Texas Instruments) with an accuracy up to ±0.1 °C and resolution of 0.0078 °C is integrated within the sensor module and monitors the skin temperature every 1 s. A low-power motion sensor (ICM-20948, TDK Corporation) records the user's linear and angular acceleration about three axes at 50 Hz, providing a set of data relevant to interpret work pattern and intensity. Next, a multiprotocol System-on-Chip module (nRF52832, Nordic Semiconductors) receives the sensor data (via SPI for ADS1292, ICM-20948 and I^2C for TMP117) and regulates circuit operation with a built-in microprocessor, processing and transmitting the data to a connected smartphone through the 2.4 GHz transceiver. An Android smartphone (Galaxy A51, Samsung) equipped with a custom application is used to continuously display sensor data for real-time monitoring of a farmworker's physiological status and store them for additional analysis. Finally, sensors and chip components are connected to the flexible printed circuit board (fPCB, PCBminions, Inc.). The first board is for sensor data management and BLE, while the second board is for power and battery management. Figure S1 illustrates the detailed flow of the sensor data acquisition and processing.

2.2. Fabrication, assembly, and physical properties of biopatch

Employing sophisticated microfabrication techniques used in CMOS manufacturing toward skin-wearable thin-film sensor electronics has demonstrated its merit through numerous healthcare applications that highlight the ability of thin films to establish conformal contact with human skin.[19–21] However, significant disadvantages include the need for a cleanroom facility and expensive equipment, low production yield due to unconventional use of equipment optimized for wafer processes, and inability for scaled manufacturing due to vacuum-based processes and a small number of devices that can fit in a wafer. More recently, advances in manufacturing technology and electronic chip packaging enabled the incorporation of miniaturized IC components with a thin electronic platform to equip modern electronic functions, such as signal processing, sensing, and wireless communication.[22–24] Efforts to enhance the manufacturability of thin, stretchable biopotential electrodes have been made, including 'upside-down' electrode deposition for direct adhesive integration,[25] electrode patterning using a silhouette cutter[26] and laser ablation.[27] However, none of these approaches demonstrated the feasibility for integration into a fully packaged wearable device, let alone validation in field studies. This study introduces the first use case of a femtosecond infrared (IR) laser micromachining system (WS-Flex, Optec), a versatile, high-precision machining tool for a wide range of materials with minimum thermal effects, to enable a high-throughput electrode and interconnect fabrication and a strategy for assembly into a wearable device. Figure 2A illustrates the overall device integration flow composed of three main steps: 1) laser cutting of electrodes

and adhesives, 2) sensor module assembly, and 3) final device integration. The starting substrate for the electrodes and interconnects is a 12.7 μm-thick polyimide sheet (50HN Kapton Film, DuPont) deposited with layers of chromium (Cr) and gold (Au) in thicknesses of 5 nm and 200 nm, respectively (Figure 2B). Being laminated on a PDMS-coated glass slide, once laser-cut, the non-functional region of the substrate can be removed by peeling. To facilitate the removal of the non-functional piece, the design avoids looped features, allowing a single-step removal process (Figure 2C). Each electrode has an overall shape of an 11.5 cm^2 square with a network of serpentine patterns, with a trace width of 0.16 mm and a bending radius of 0.39 mm. Stretchable interconnect traces with the same serpentine design elements are extended from the electrodes to facilitate connection to the module and are coated with a layer of a low modulus elastomer (Ecoflex Gel, Smooth-On) to provide insulation and adhesion (Figure 2D). Similarly, the medical adhesive is laser-cut to form both the main electrode adhesive and protective cover. The electrodes are transferred to the adhesive side of the medical adhesive using a water-soluble tape (ASWT-2, AQUASOL), following the procedure described in our previous works.[19, 28] Surface mount chip components are soldered to the two 2-layer fPCB using reflow soldering with a solder paste (SMDLTLFP10T5, Chip Quik), while the two boards and a battery are interconnected with Cu wires (Figure S2). The fPCB and electrodes are electrically connected by bonding flexible film wires (HST-9805-210, Elform) with silver paint (Fast Drying Silver Paint, Ted Pella), followed by encapsulation with elastomer (Ecoflex 0030, Smooth-On). Details of the wire connection and encapsulation processes are shown in Figure S3. Finally, a layer of silicone elastomer (Ecoflex 0030, Smooth-On) is coated around the electronics to provide protection against environmental elements, such as dust, particles from crops, and contacts with clothing and tools. The module and substrate are bonded with an adhesive (Sil-Poxy, Smooth-On), let cured at room temperature for one day for permanent bonding. (Detail fabrication and assembly processes are described in the Experimental Section and Figure S4.)

2.3. Stretchability and integrity over repeated stress

The combination of the serpentine design concept and the elasticity of the medical tape allows the biopatch to be overall stretchable. Though the chest area does not exhibit significant skin strain, specific tasks involving the movement of both arms and torso may create significant strain. Here, we conduct a set of experimental investigations to understand the maximum stretchability of the device using abrupt changes in the electrical resistance as the measure of failure. Samples of the biopatch were mechanically stretched using a motorized test stand (ESM303, Mark-10) while the resistance of the two furthest points in the electrode layer is measured using a digital multimeter (DMM7510, Keithley Instruments). As shown in Figure 2E, a fully integrated biopatch was able to stretch by 30%, which far exceeds the physiological relevance, without experiencing a fracture in the Au trace or other structural failure.[29] Electrically, the Au layer, which has been modified to form a continuous conductive pathway between two furthest electrodes for this test (Figure S5), showed a negligible change in resistance with an increase of 1.83 Ω, or 0.56% of its original value (Figure 2F). Agricultural work involves repetitive arm and torso movement. Thus, an investigation of the long-term stability of the biopatch is needed. The test was set up to stretch and relax the device cyclically by 15% for 500 cycles. The experimental

result revealed the biopatch's ability to withstand extreme cases of skin deformation up to 15%, far beyond expected skin strains in the chest area.[29] As shown in Figure 2G, the electrode layer's resistance showed a negligible long-term change before and after the test with a decrease of 1 Ω, or 0.30%. For each stretching cycle, a maximum change in resistance of 0.62 Ω, or 0.18%, was measured, indicating the robustness of the adhesive-integrated, laser-cut electrodes as well as the overall device against large and repeated mechanical stretching. Though the fPCBs contained in the sensor are flexible, their mechanical limit must be verified. As shown in Figure 2H, the main sensor fPCB is positioned between a flat sample stage and a V-shaped groove and compressed using ESM303. The circuit was connected to a smartphone to inspect sensor data recorded during the tests (Figures 2I and 2J). A detailed view of the setup is shown in Figure S6a. Resistance across two furthest ground nodes measured by the multimeter showed a decrease by 0.026 Ω, or 0.49%, which has a negligible effect on circuit operation. After 500 cycles of bending, the circuit's resistance showed a slight decrease in the overall resistance by 1.23 Ω, or 0.23%. Sensor data acquired during the cyclic bending test showed no effect from bending, evidenced by the stable BLE connection, data transfer rate, and continuous sensor (motion) data (Figure S6b). The collective results from stretching and bending experiments prove that the biopatch should serve as a robust hardware platform with a capacity to withstand long-term bending and stretching.

2.4. Evaluation of biopatch adhesion in high sweat and heat conditions

As with most medical adhesives, the biopatch's adhesive substrate (9907T) is part of the pressure-sensitive adhesives (PSAs) family, with an acrylic layer serving as the adhesive material.[30] Since PSAs rely solely on the van der Waals interactions between the skin and the polymer matrix, maintaining adhesion during prolonged wear is speculated to be affected by moisture at the interface.[31, 32] Therefore, maintaining a dry skin-adhesive interface by the removal of moisture is vital for retaining the tape-skin adhesion, and consequently, the electrode-skin adhesion. Moisture vapor transmission rate (MVTR) is an experimentally determined value describing a material's ability to transfer water through its thickness and is often specified for commercial medical adhesives. 3M provides 9907 T's MVTR information; however, it is listed as a range expression of > 4000 $g/m^2/day$ and requires validation of the material's effectiveness in maintaining skin adhesion in the presence of excessive sweat. To experimentally determine the MVTR value of 9907T and other materials, we prepared glass bottles. Their openings were covered with 9907T, 2476P, Tegaderm, Ecoflex, and PDMS. Ecoflex represents the mixture of Ecoflex 0030 and Ecoflex Gel in a 1:1 weight-ratio, and the thickness of both Ecoflex and PDMS was 0.5 mm. The sixth bottle without any cover was prepared as a reference. Next, the weight of each bottle was measured every 3 hours over 24 hours at room temperature. Detail experimental setup is shown in Figure S7. As shown in Figure 3A, the MVTR value determined for 9907T was 40.28 $g/m^2/hr$, equating to 966.72 $g/m^2/day$. Though this is far less than the manufacturer's stated value, the MVTR result depends heavily on the experimental setup and meaningful conclusions, such as the relative value to the open-bottle measurement. In this test, the 9907T bottle could transmit 46% of total water evaporated from the open bottle and performed far superior to other materials.

We conducted an in vivo test, where the contact qualities of 9907T in the chest area were determined based on peel forces and SNR of ECG. As shown in Figure 3B, an adhesive containing ECG electrodes was attached in the same manner as the biopatch is used, while a set of three samples with an attachment area of 2×2 cm^2 was attached below the sternal region. The tip of the peel test sample was attached to a digital force gauge (M5-5, Mark-10) by looping it around the gauge's hook attachment. The paper liner prevented sticking of the area beyond the intended attachment area. To vary the level of skin perspiration, the subject was asked to perform a series of physical exercise, including 20 squats, a 1-min plank, and 10 push-ups without a break. Immediately following the exercise, the level of perspiration at the sternum was measured using a skin hydration sensor (MoistureMeterSC, Delfin Technologies), followed by a 5-min ECG collection for SNR analysis (Figure 3C). A detailed view of the measurement setup is shown in Figure 3D. For quantifiable evaluation of adhesion, the force gauge connected to an adhesive sample is pulled perpendicularly from the chest while the time-force data were saved to a computer via a wired connection (Figure 3E). Figure 3F shows peel force data collected with three samples at a particular skin hydration level, with each of the three curves representing a record of force-time data until complete detachment. Here, the total energy required to fully detach a sample is assessed by calculating the area under the curve using a trapezoidal rule using MATLAB, and, for each hydration level, average peel energy is calculated (Figure S8a). Full results, including the force-time curves and calculated areas for all hydration levels are shown in Figure S8b. ECG collected immediately after the peel tests were analyzed for its SNR using a variation of Pan-Tompkins algorithm that inspects the data in 30-sec windows and the representative SNR was determined by finding the average SNR over the 2 min-long ECG data (Figure S9). As shown Figure 3G, initially, the peel energy over increasing sweat levels shows a decreasing trend from 617.2 but approaches a stable value of 317.5 at the highest sweat level. On the other hand, a positive trend in SNR is observed due to the lowered skin-electrode impedance from sweat,[33]. However, the value decreased at the maximum sweat level due to weakened electrode adhesion caused by excessive sweat. Despite the decrease at the end, all SNR values recorded higher than 20dB, which exceeds the SNR threshold that guarantees the preservation of ECG features (PQRST) and accurate HR extraction based on our prior works.[19, 34, 35]

Next, considering the normal maximum ambient temperature in August between 1990 and 2020 for intended test sites (Volusia County, Florida) is 32.1 °C, the biopatch's ability to operate in a hot environment was verified by putting the device in an oven set at 60 °C for 1 hour (Figure 3H). The Android application was modified to write a Bluetooth data transfer rate, which serves as an indirect measure of normal circuit functions. Figure 3I shows that the temperature sensor data recorded by the biopatch accurately tracked the temperature changes between the room and oven, while the data transfer rate remained stable at 752 kB/s, regardless of the location. Collectively, the set of experimental data presented here demonstrates the structural and functional integrity of the biopatch for robust operation in high sweat and heat environments.

2.5. Evaluation of biopatch's sensing performance

Having verified its structural integrity and functional robustness in simulated experiments and analysis, sensor performance comparison between the biopatch and a set of standard health monitoring equipment was conducted. As illustrated in Figure 4A, a healthy male subject was equipped with a chest strap HR monitor (Polar T31, Polar Electro), an accelerometer (GTX3+, ActiGraph) on the waist, and an ambient temperature sensor (iButton, DS1923-F5#, iButtonLink) hung on the belt at the waist, following the same protocol used in a previous pilot study conducted in 2012 and 2013.[12] The subject was administered with an ingestible temperature sensor (CorTemp Ingestible Core Body Temperature Sensor, HQInc.) 12 hours prior to the experiment to allow the pill sensor to arrive at the lower digestive tract. To evaluate the capacity of the biopatch's integrated motion sensor (with a 50 Hz sampling rate), the subject performed a set of simulated tasks, such as lifting an object from the floor, climbing a ladder, and placing an object on a shelf. Each task was performed repeatedly without a break for 2 minutes with 1-minute beaks between tasks. Though GTX3+, the counterpart motion sensor, was configured to record triaxial acceleration at a 50 Hz sampling rate, the proprietary software (ActiLife) converted the raw data into 10-seconds epoch-level activity counts, the values of which are combined to produce a one-dimensional value known as Vector Magnitude (VM). As shown in Figure 4B, both the biopatch and GTX3+ detected the start and end of each task. However, due to the nature of epoch-level resolution, GTX3+ showed delayed responses to subject's motion. Similarly, quantification of activity as epoch-level data and VM conversion inevitably reduced the amount of information typically offered by modern motion sensors. Specifically, zoomed plots of the biopatch's motion data show that individual tasks, such as climbing the ladder up and down (colored in red and blue, respectively), can be distinguished, whereas GTX3+ provides one VM data point for every 10 seconds. Next, the biopatch's comprehensive sensing capability in an outdoor setting was evaluated by requesting the subject to perform 3 min-long squat exercises three times with 1 min breaks in between. The protocol was conducted at a local park on a sunny day at three separate times—6:30 AM, 11:00 AM, and 3:00 PM. Figure 4C presents a 15-minute snapshot of all data collected by both the biopatch and comparison devices during the 11:00 AM trial. Noteworthy results include successfully capturing the rise in HR, skin temperature, and T_c in response to exercise, along with a high correlation between the two HR data. Details of the methodology for HR is described in the Experimental Section and Figure S10. T_c continuously increased from 37.63 °C to 37.93 °C during both exercise and resting periods. Such rise of T_c during a resting period is expected considering that T_c is a result of combined effects of thermoregulation and environmental factors.[36] Figure 4D shows HR data from the biopatch and Polar during the 20 minute-long 11:00 AM protocol composed of 3 sets of squats, where biopatch's HR curve can be seen aligned with Polar's HR datapoints. Using statistical techniques, the robustness of the biopatch's HR was evaluated. First, as shown in Figure 4E, the result of the correlation analysis shows a highly linear relationship with the correlation coefficient (r) of 0.99 and the coefficient of determination (r^2) of 0.98. Next, the Bland-Altman plot was used to describe the level of agreement between the two HR data. As shown in Figure 4F, the mean bias between the two sets of HR data is 0.04 and 95% of all differences fall between +6.3 (+1.96 SD) and −6.3 (−1.96 SD). Similar levels of linear correlation and agreement between the biopatch and Polar HR data are observed

in both the 6:30 AM and 3:00 PM trials, indicating the robustness of the biopatch as an outdoor HR monitor (Figure S11). Finally, the average SNR values between two activity states from the 3:00 PM protocol were calculated to be 25.00 dB and 19.88 dB, respectively. This result confirms that high-fidelity ECG data could be recorded even during intense physical activities (Figure S12a). Qualitative inspection of the raw ECG over a 10-sec window during a period of elevated activities further indicates that no significant degradation in the waveform is noticed, aside from the increase in HR and the slight increase in the baseline fluctuation due to device's inertial forces acting on the skin (Figure S12b).

2.6. Deploying biopatch for health monitoring of agricultural workers

Finally, to verify the utility of the biopatch as a reliable health monitoring device in agricultural settings, agricultural workers from two communities in northeast Central Florida (Apopka and Pierson) were recruited in July 2021 to conduct a field-based health monitoring study. In particular, the study sites represented environmental factors known to endanger outdoor workers, such as elevated temperature, humidity, solar radiation, and diminished air circulation.[37] As shown in Figure 5A, the biopatch was applied to the participant's chest at the beginning of the workday, along with the conventional monitoring setup described earlier. Once equipped with the devices, each participant proceeded to worksites to perform tasks relevant for three agricultural work types: ferneries, nurseries, and field crops. At the end of the workday, the participants returned to the field office to remove the biopatch and return other devices. Visual inspection verified that all biopatches maintained good adhesion to the skin and showed no visible damages, with only two devices showing the cover layer partially removed due to excessive rubbing of the clothes (Figure S13). Table 1 compares our work with recent studies within the scope of occupational health monitoring based on wearable sensors.

For all participants, the removal process of the biopatch initially caused mild skin redness due to the tension caused by pulling the tape but it disappeared in a few minutes. No negative skin reaction was observed (Figure 5B). As described previously, the biopatch's robustness in long-term skin adhesion can be quantitatively evaluated by inspecting the quality of the recorded ECG. Therefore, the average SNR of the 3 min-long ECG segment at the start, middle, and end of the workday were calculated and plotted to inspect wear-time-dependent variation in SNR. Figure 5C shows the continuous 6 hour-long ECG collected during a participant's (Participant 2) workday, indicative of robust operation of the biopatch regardless of the time of the workday. Closer inspection (6 sec windows) within the three 3 min-long ECG segments reveals that detailed ECG features are preserved at all three phases and based on the values of SNR, no apparent wear time-dependent skin-electrode contact degradation is observed. Results of the same analysis for five additional participants show that ECG data from all participants have SNR greater than 20 dB, indicating reliable biopatch adhesion to the skin, independent of the phase of workday or the type of work performed. In general, SNR values increased as the wear time progressed, which can be explained by improved electrical and mechanical contact mediated by the ionic components of sweat and sweat's physical volume that further closes the gap between the skin and thin-film electrodes. Though Participant #6's SNRs appear to show an always decreasing trend, the initial SNR showed an exceptionally high value of 43.06 dB, which may be due

to existing sweat or remaining moisture on the skin from recent showering (Figure 5D). With the high quality of ECG determined for the participants, the accuracy of HR estimated from field-collected ECG was inspected next. Figure 5E shows the two overlaid HR data measured from Participant 1 during the 11 hour-long field works, where the blue curve and the orange dots represent the HR measured by the biopatch and Polar, respectively. The two data show a high agreement qualitatively, and the 20 min-wide zoomed-in sections (top of Figure 5E) also reveal that the biopatch's HR traces Polar's HR closely at all recording phases. For quantitative measurement of agreement between the two HR dataset over the course of workday, linear correlation and Bland-Altman analyses were performed over hourly segmented data. The results reveal that at hours 1, 6, and 10, the two data are not only highly correlated but also show good agreement. A complete list of the analyses for the 11-hour data is shown in Table S1. Over the 11 segments, the average values for r and r^2 were 0.89 and 0.65, respectively, and those for mean bias, +1.96SD, and −1.96 SD, were 0.04, +8.1, and −8.0 BPM, respectively. Figures 5F–H show the set of activity and temperature data time-synchronized to the cardiac activity of Participant 1. Figure 5F shows the continuous 3-axis acceleration recorded by the biopatch and VM recorded by GT3X+. Both devices maintained robust functionality throughout the workday and captured various levels of activity without failure. Interestingly, the periods of reduced activity captured in both data (colored in green) are followed by a decrease in HR, verifying the biopatch's capacity to relate HR dynamics to worker's physical activities. The continuous skin and ambient temperature data are shown in Figure 5G. Though the recorded span of temperature variation was narrower for the skin, the biopatch could detect rises in the skin temperature due to the sharp rises in the ambient temperature, caused by direct exposures the sunlight, measured at around the 4^{th} and 6^{th} hours of the workday (red arrows). Interestingly, starting at hour ~6.5, the ambient temperature measured by the iButton decreased and remained below the skin temperature by approximately 5 °C. This may be due to the participant entering an area with more shades and/or increased airflow. Finally, the T_c measured by the ingestible pill sensor is shown in Figure 5H, in which intermittent interruptions in the data can be seen for up to the seventh hour and an eventual loss of data afterward. Loss of data is due to the loss of wireless connectivity between the pill sensor and the waist-worn receiver unit operating at 262 kHz. In addition, T_c datapoints beyond physiological relevance are seen scattered around the baseline data, lowering the monitoring accuracy. This artifact is due to a combined effect of RF absorption by the adipose tissues around the waist and a circuit design that fails to prevent data oscillation caused by the reduced RF performance. This is evidenced by a separate study, which observed such erratic behavior for participants with larger BMI.[38] In fact, of all six participants, from whom the biopatch successfully collected high-quality data, only Participant 2 produced a reliable T_c reading while the rest suffered from the artifact on more than 50% of the data length, with Participants 5 and 6 completely missing the T_c data. Varying degrees of such scattering artifact were observed in the rest of CorTemp's HR data with Participant #5's data suffering the most. Figure S14 summarizes the overall data integrity of all participant data.

3. Conclusion

This paper reports a soft wireless chest-wearable patch for accurate physiological monitoring of farmworkers, an occupational group exposed to an increased risk of HRI and deaths due to climate change and lack of safety mandates. A comprehensive set of study results, including adhesion, mechanics, breathability, along with a successful collection of field data, indicates that the biopatch can serve as a reliable health monitor for agricultural workers. Validation of high-fidelity long-term ECG based on SNR analysis confirms the robust skin-device interface despite harsh environmental factors as well as the user's perspiration throughout the workday. Furthermore, the successful collection of continuous skin temperature and activity data demonstrates the biopatch's function to conduct multi-parameter physiological monitoring with a single device. Future study plans a larger-scale field data collection with farmworkers in the real-time detection of HRI using a machine learning algorithm. Finally, the presented biopatch will enable quantifiable assessment of farmworkers' physiological status, establishing evidence-based safety standards for outdoor workers and the agricultural industry.

4. Experimental Section

Electrode substrate preparation:

A clean glass slide is spin-coated with PDMS (Sylgard 184, Dow) mixed in a 1:10 curing agent to base ratio. 12.7 μm-thick polyimide sheet (50HN Kapton Film, DuPont) is laminated onto the PDMS-coated glass slide and Cr and Au layers are deposited in thicknesses of 5 nm and 200 nm, respectively, using an electron beam deposition tool (Denton Explorer). Next, a femtosecond IR laser micromachining tool (WS-Flex, Optec) is used to pattern the metal-Kapton laminate with laser power at 50 W and pattern repetition cycles of two. With the non-functional piece is removed, water-soluble tape (ASWT-2, AQUASOL) is used to transfer the functional piece from the PDMS/glass substrate to the adhesive side of 9907T. Once the water-soluble tape is removed and the sample is dried, a low modulus elastomer (Ecoflex GEL, Smooth-On) is applied along the interconnect lines and cured at room temperature for 1 hour for insulation without sacrificing overall adhesiveness. Illustrations in Figure S3 describe this process in detail.

Wireless sensor module assembly and biopatch integration:

Surface mount chip components are soldered to the two 2-layer fPCBs using reflow soldering with a solder paste (SMDLTLFP10T5, Chip Quik), by using a hot plate set at 100 °C and ramping to 150 °C in a 10 °C increment every 1 minute. Cu wires are soldered to interconnect the two fPCBs, the rechargeable lithium-ion polymer battery (105 mA, LP401230, Adafruit), a slide switch, and a magnetic adapter. The switch and the magnetic adapter are fixed to the battery using a two-part epoxy (ClearWeld, JB Weld) and curing for 24 hours. A layer of silicone elastomer (Ecoflex 0030, Smooth-On) prepared and mixed with coloring pigment (Silc Pig™, Smooth-On) casted over the electronics, while leaving the sensor connection pads exposed, followed by curing in a vacuum oven set at 60 °C for 1 hour. The insulated module and the electrode substrate are bonded with a one component adhesive (Sil-Poxy, Smooth-On), let cured at room temperature for 1 day for permanent

bonding. Flexible film wires (HST-9805-210, Elform) are used to electrically connect the electrodes and the wireless module using silver paint (Fast Drying Silver Paint, Ted Pella). Finally, the connection is sealed with Ecoflex 0030 used in the previous step. Details of the film wire connection and insulation are shown in Figure S3.

HR estimation method:

Spurious peaks were discarded using a custom thresholding algorithm. First, the filtered ECG signal was squared and smoothed with a wide (one hundred samples) Gaussian, resulting in an attenuated envelope of the squared signal. MATLAB's findpeaks function was used on the smoothed result, with interpolation between the found peaks forming a dynamic threshold. To account for a variety of noise levels, a vertical offset at each interpolated threshold value was found by adding a short moving average of recent filtered ECG values with a user-controlled coefficient to the square root of each threshold value. Finally, every peak was included if its filtered ECG amplitude was above the threshold and discarded otherwise. With most of the incorrectly found peaks found and removed, counting progressed according to the following logic: first, check the amount of time since the previous peak and calculate a nominal heart rate of sixty divided by this period. If the time since the last beat is otherwise physiologically unreasonable (greater than one second or less than 0.33 seconds), record a short moving average of past values (i.e., excluding the calculated nominal heart rate) for this peak. If the heart rate is physiologically reasonable but has changed significantly since the last recorded value, record a short moving average including the nominal heart rate. Finally, if none of the above holds, simply record the heart rate at this peak as the nominal value originally calculated. The found heart rate values were then smoothed using a Gaussian of user-controlled size.

Human subject study:

The human pilot study involved multiple healthy volunteers; the study followed the approved IRB protocol from Emory University (# MOD005-IRB00112681). All participants agreed and signed the consent form to allow the experiment procedure.

Statistical analysis:

All statistical analyses were performed using MATLAB software. Data shown in Figure 3G and Figure 5D were presented as mean ± SD (n = 3 and 5 for Figure 3G and 5D, respectively). For all Bland-Altman plots, dashed lines indicate ± 1.96 SD while the center solid line represents the mean bias value.

Supplementary Material

Refer to Web version on PubMed Central for supplementary material.

Acknowledgements

We acknowledge the support of the IEN Center Grant (Center for Human-Centric Interfaces and Engineering) from the Georgia Tech Institute for Electronics and Nanotechnology. This work was performed at the Georgia Tech Institute for Electronics and Nanotechnology, a member of the National Nanotechnology Coordinated Infrastructure (NNCI), which is supported by the National Science Foundation (ECCS-1542174). The authors would also like to acknowledge the study participants for their time and participation.

References

[1]. Gubernot DM, Anderson GB, Hunting KL, Int. J. Biometeorol 2014, 58, 1779. [PubMed: 24326903]

[2]. Luginbuhl RC, Jackson LL, Castillo DN, Loringer KA, JAMA J Am. Med. Assoc 2008, 300, 1017.

[3]. Gubernot DM, Anderson GB, Hunting KL, Am. J. of Ind. Med 2015, 58, 203. [PubMed: 25603942]

[4]. Flouris AD, Dinas PC, Ioannou LG, Nybo L, Havenith G, Kenny GP, Kjellstrom T, Lancet Planet. Health 2018, 2, E521. [PubMed: 30526938]

[5]. Hansen J, Sato M, Ruedy R, Proc Natl Acad Sci U S A 2012, 109, E2415. [PubMed: 22869707]

[6]. CDC, Heat Stress, https://www.cdc.gov/niosh/topics/heatstress/default.html, accessed: Februray, 2022.

[7]. OSHA, Overview: Working in Outdoor and Indoor Heat Environments, https://www.osha.gov/heat-exposure, accessed: Februray, 2022.

[8]. NFPA, Standard on the Rehabilitation Process for Members During Emergency Operations and Training Exercises, https://www.nfpa.org/codes-and-standards/all-codes-and-standards/list-of-codes-and-standards/detail?code=1584, accessed: February, 2022.

[9]. Morrissey MC, Wu Y, Zuk EF, Livingston J, Casa DJ, Pescatello LS, J. Sci. Med. Sport 2021, 24, 843. [PubMed: 34175202]

[10]. Morrissey MC, Brewer GJ, Williams WJ, Quinn T, Casa DJ, Am. J. Ind. Med 2021, 64, 981. [PubMed: 34590324]

[11]. Morrissey MC, Casa DJ, Brewer GJ, Adams WM, Hosokawa Y, Benjamin CL, Grundstein AJ, Hostler D, McDermott BP, McQuerry ML, Stearns RL, Filep EM, DeGroot DW, Fulcher J, Flouris AD, Huggins RA, Jacklitsch BL, Jardine JF, Lopez RM, McCarthy RB, Pitisladis Y, Pryor RR, Schlader ZJ, Smith CJ, Smith DL, Spector JT, Vanos JK, Williams WJ, Vargas NT, Yeargin SW, GeoHealth 2021, 5, e2021GH000443.

[12]. Mac VVT, Tovar-Aguilar JA, Flocks J, Economos E, Hertzberg VS, McCauley LA, J. Agromedicine 2017, 22, 89. [PubMed: 28118110]

[13]. Mac V, Elon L, Mix J, Tovar-Aguilar A, Flocks J, Economos E, Hertzberg V, McCauley L, J. Occup. Environ. Med 2021, 63, 395. [PubMed: 33560064]

[14]. Mac VV, Elon L, Smith DJ, Tovar-Aguilar A, Economos E, Flocks J, Hertzberg V, McCauley L, Am. J. Ind. Med 2021, 64, 258. [PubMed: 33543496]

[15]. Trung TQ, Lee NE, Adv. Mater 2016, 28, 4338. [PubMed: 26840387]

[16]. Jin H, Abu-Raya YS, Haick H, Adv. Healthc. Mater 2017, 6, 1700024.

[17]. Khan Y, Ostfeld AE, Lochner CM, Pierre A, Arias AC, Adv. Mater 2016, 28, 4373. [PubMed: 26867696]

[18]. Jeong H, Lee JY, Lee K, Kang YJ, Kim JT, Avila R, Tzavelis A, Kim J, Ryu H, Kwak SS, Kim JU, Banks A, Jang H, Chang JK, Li S, Mummidisetty CK, Park Y, Nappi S, Chun KS, Lee YJ, Kwon K, Ni X, Chung HU, Luan H, Kim JH, Wu C, Xu S, Banks A, Jayaraman A, Huang Y, Rogers JA, Sci. Adv 2021, 7, eabg3092.

[19]. Kim Y-S, Mahmood M, Lee Y, Kim NK, Kwon S, Herbert R, Kim D, Cho HC, Yeo W-H, Adv. Sci 2019, 6, 1900939.

[20]. Kim D-H, Lu N, Ma R, Kim Y-S, Kim R-H, Wang S, Wu J, Won SM, Tao H, Islam A, Yu KJ, Kim T.-i., Chowdhury R, Ying M, Xu L, Li M, Chung HJ, Keum H, McCormick M, Liu P, Zhang Y-W, Omenetto FG, Huang Y, Coleman TP, Rogers JA, Science 2011, 333, 838. [PubMed: 21836009]

[21]. Kim H, Kim Y-S, Mahmood M, Kwon S, Zavanelli N, Kim HS, Rim YS, Epps F, Yeo W-H, Adv. Sci 2020, 7, 2000810.

[22]. Kim Y-S, Lu J, Shih B, Gharibans A, Zou Z, Matsuno K, Aguilera R, Han Y, Meek A, Xiao J, Tolley MT, Coleman TP, Adv. Mater 2017, 29, 1701312.

[23]. Kim J, Salvatore GA, Araki H, Chiarelli AM, Xie ZQ, Banks A, Sheng X, Liu YH, Lee JW, Jang KI, Heo SY, Cho K, Luo HY, Zimmerman B, Kim J, Yan LQ, Feng X, Xu S, Fabiani M, Gratton G, Huang YG, Paik U, Rogers JA, Sci. Adv 2016, 2, e1600418. [PubMed: 27493994]

[24]. Lee SP, Ha G, Wright DE, Ma Y, Sen-Gupta E, Haubrich NR, Branche PC, Li W, Huppert GL, Johnson M, Mutlu HB, Li K, Sheth N, Wright JA Jr., Huang Y, Mansour M, Rogers JA, Ghaffari R, npj Digit. Med 2018, 1, 2. [PubMed: 31304288]

[25]. Kang DY, Kim Y-S, Ornelas G, Sinha M, Naidu K, Coleman TP, Sensors 2015, 15, 23459. [PubMed: 26389915]

[26]. Yang SX, Chen YC, Nicolini L, Pasupathy P, Sacks J, Su B, Yang R, Sanchez D, Chang YF, Wang PL, Schnyer D, Neikirk D, Lu NS, Adv. Mater 2015, 27, 6423. [PubMed: 26398335]

[27]. Chae H, Kwon HJ, Kim YK, Won Y, Kim D, Park HJ, Kim S, Gandla S, ACS Appl. Mater. Interfaces 2019, 11, 28387. [PubMed: 31294964]

[28]. Kim Y-S, Basir A, Herbert R, Kim J, Yoo H, Yeo W-H, ACS Appl. Mater. Interfaces 2020, 12, 3059. [PubMed: 31842536]

[29]. Wessendorf AM, Newman DJ, IEEE Trans. Biomed. Eng 2012, 59, 3432. [PubMed: 22961262]

[30]. Czech Z, Kurzawa R, J. Appl. Polym. Sci 2007, 106, 2398.

[31]. Eiler J, Hansen D, Bingol B, Hansen K, Heikenfeld J, Thormann E, Int. J. Adhes. Adhes 2020, 99, 102574.

[32]. Renvoise J, Burlot D, Marin G, Derail C, J. Adhesion 2007, 83, 403.

[33]. Kalevo L, Miettinen T, Leino A, Kainulainen S, Korkalainen H, Myllymaa K, Töyräs J, Leppänen T, Laitinen T, Myllymaa S, IEEE Access 2020, 8, 50934.

[34]. Rodeheaver N, Herbert R, Kim YS, Mahmood M, Kim H, Jeong JW, Yeo W-H, Adv. Funct. Mater 2021, 31, 2104070.

[35]. Kim Y-S, Mahmood M, Kwon S, Maher K, Kang JW, Yeo W-H, IEEE Trans. Biomed. Eng 2019, 67, 2159. [PubMed: 31794383]

[36]. Gleeson M, Int J Sports Med 1998, 19, S96. [PubMed: 9694408]

[37]. Flocks J, Vi Thien Mac V, Runkle J, Tovar-Aguilar JA, Economos J, McCauley LA, J. Agromedicine 2013, 18, 350. [PubMed: 24125050]

[38]. Monnard CR, Fares EJ, Calonne J, Miles-Chan JL, Montani JP, Durrer D, Schutz Y, Dulloo AG, Front. Endocrinol 2017, 8, 130.

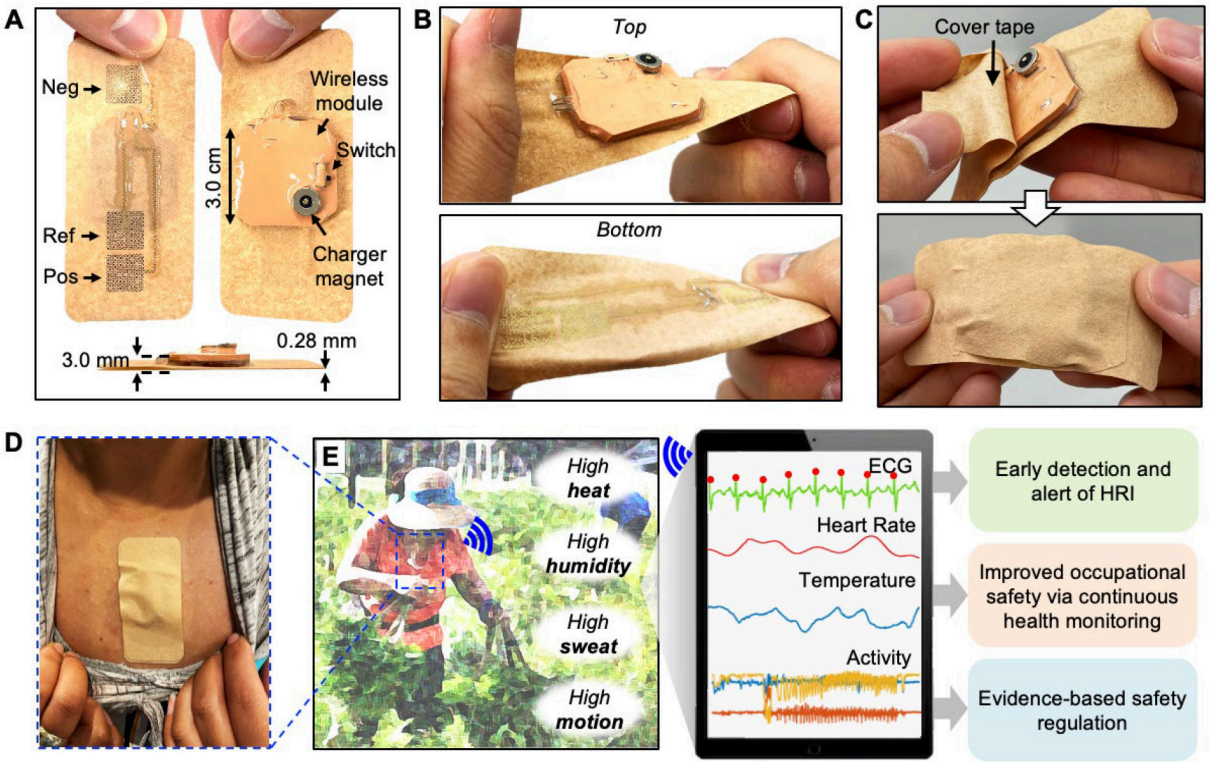

Figure 1. Overview of the device design and functionality.

(A) Photo of a fabricated bioelectronic system (biopatch) with top, bottom, and side views, showing the electrode configuration, system components, and form factor. (B) Stretchable and twistable biopatch that is integrated with a breathable substrate. (C) Before mounting the device on a farmer's skin, a thin cover tape is applied to protect it from dust, rain, and rubbing. (D) Biopatch mounted on the chest. (E) Biopatch's functionality to detect heart functions, temperature, and motion of farmworkers, which are used for HRI monitoring.

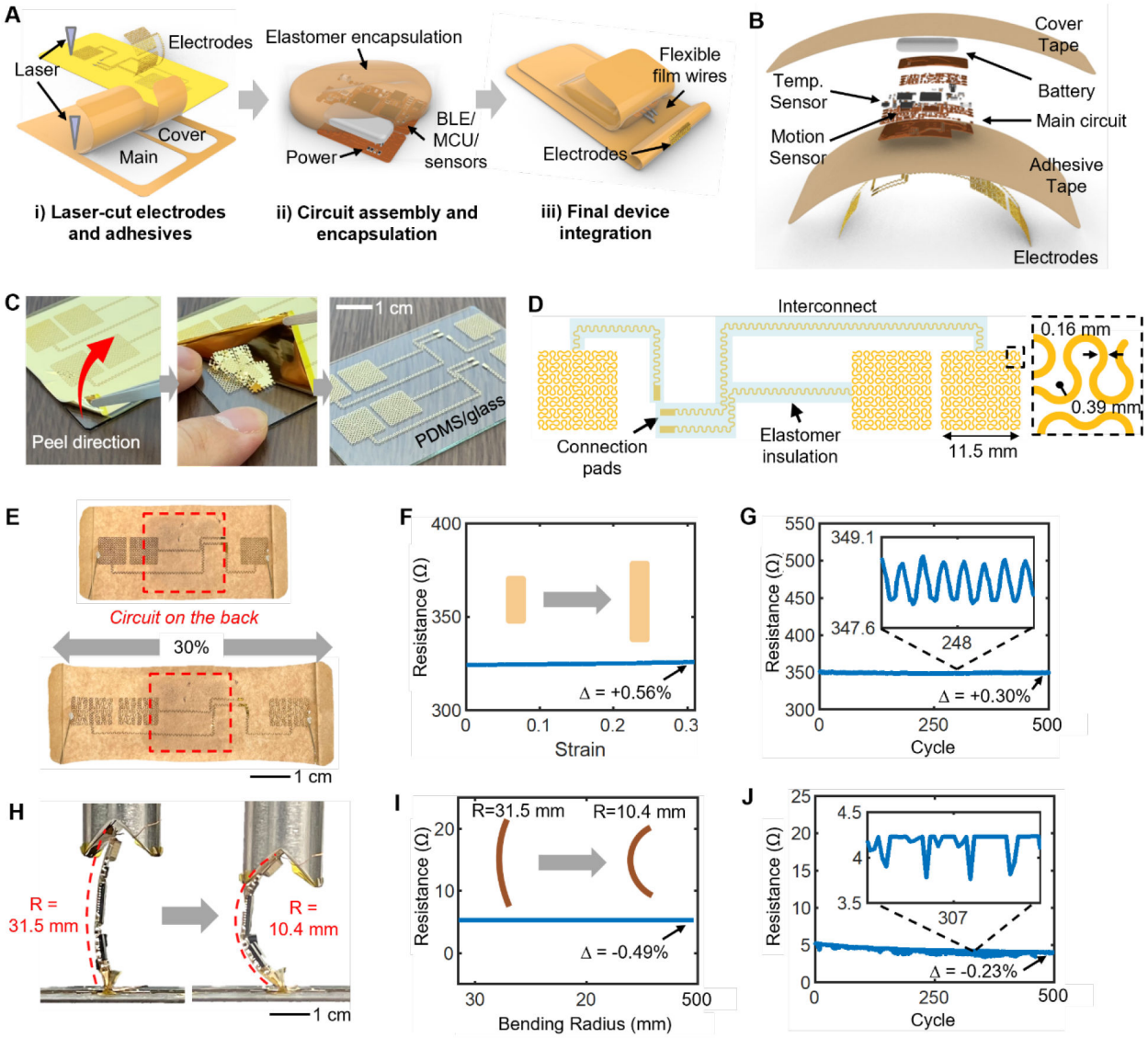

Figure 2. Fabrication of a biopatch and mechanical reliability.

(A) Schematic illustration of the three main steps involved with biopatch assembly. (B) Blowup render of the biopatch detailing the stacking order of various components. (C) Single-step removal of the non-functional region of the laser-cut film and leaving the functional electrodes. (D) Drawing of the electrode-interconnect showing the serpentine traces and areas insulated with an elastomer. (E) Experimental validation of the maximum stretchability of the electrodes. (F–G) Measured resistance across the two furthermost electrodes during full stretching (F) and cyclic stretching (G). Relative values of resistance (Δ) show negligible changes. (H) Experimental bending analysis for the wireless circuit (R=radius of curvature). (I–J) Measured resistance across two furthermost points on the circuit's ground node during maximum bending (I) and cyclical bending (J) tests.

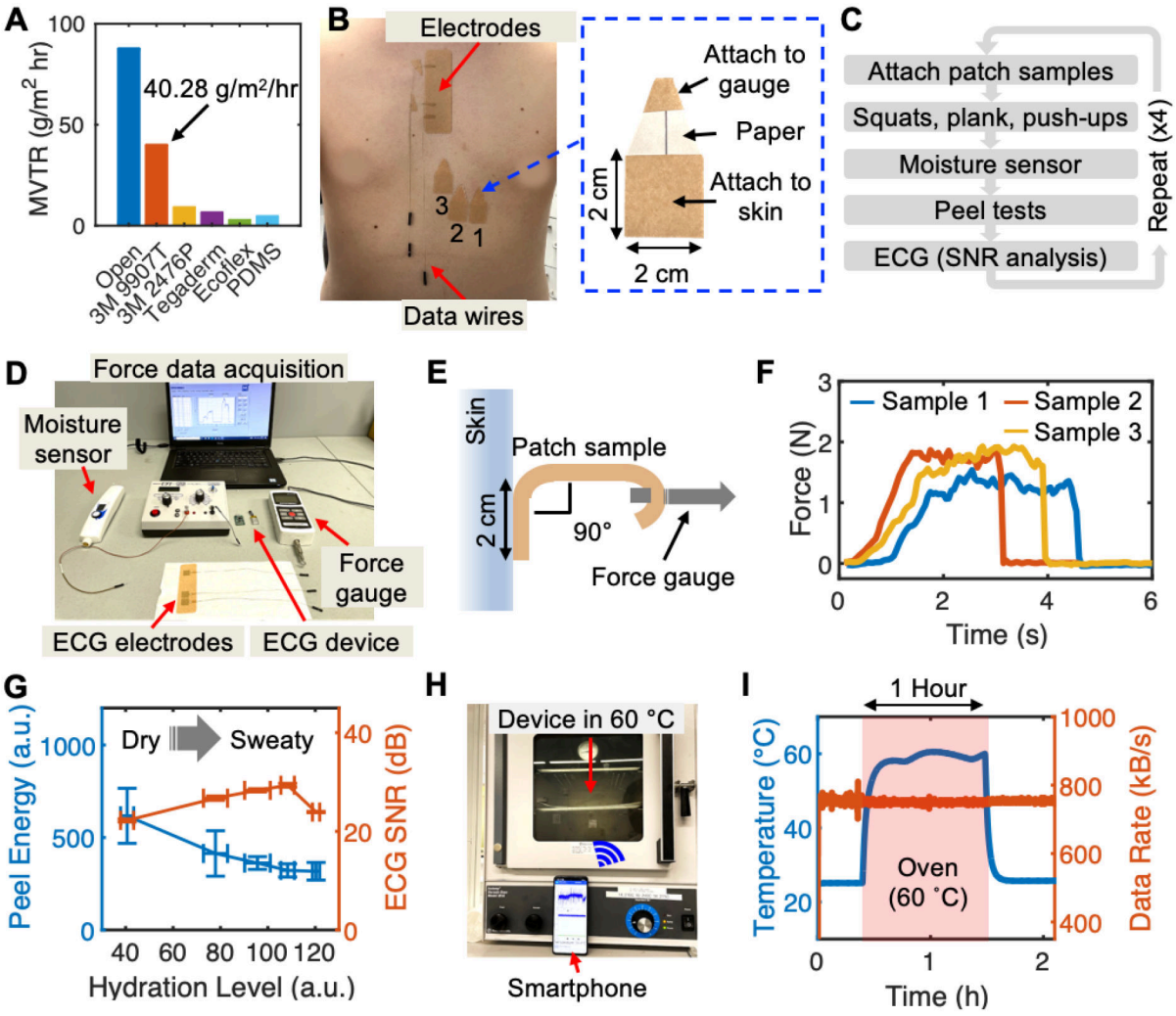

Figure 3. Robustness of biopatch in high sweat and heat conditions.

(A) Experimentally measured MVTR values for 9907T tape (orange bar) and other materials. (B) Experimental validation of electrode adhesion to the skin in high sweat conditions; electrodes on the chest for ECG recording and three blank square tapes for peel force measurement. Inset photograph details the 2 cm × 2 cm attachment area and the extension at the top for force gauge attachment. (C) Experimental protocol for electrode adhesion test. (D) Experimental setup for the adhesion test. (E) Peeling of a sample using a hand-held force gauge. (F) Force-time curves generated by peeling samples until full detachment. The area under the curve is used to quantify the total energy. (G) Calculated average peel energy and SNR of ECG over increasing skin hydration levels. Data are mean ± SD (n = 3). (H) Testing biopatch functionality in a high heat setting at 60 °C and transmitting sensor data to a smartphone. (I) Temperature (blue) recorded by the biopatch during the high heat test and the data transfer rate (orange) as an indication for normal circuit operation.

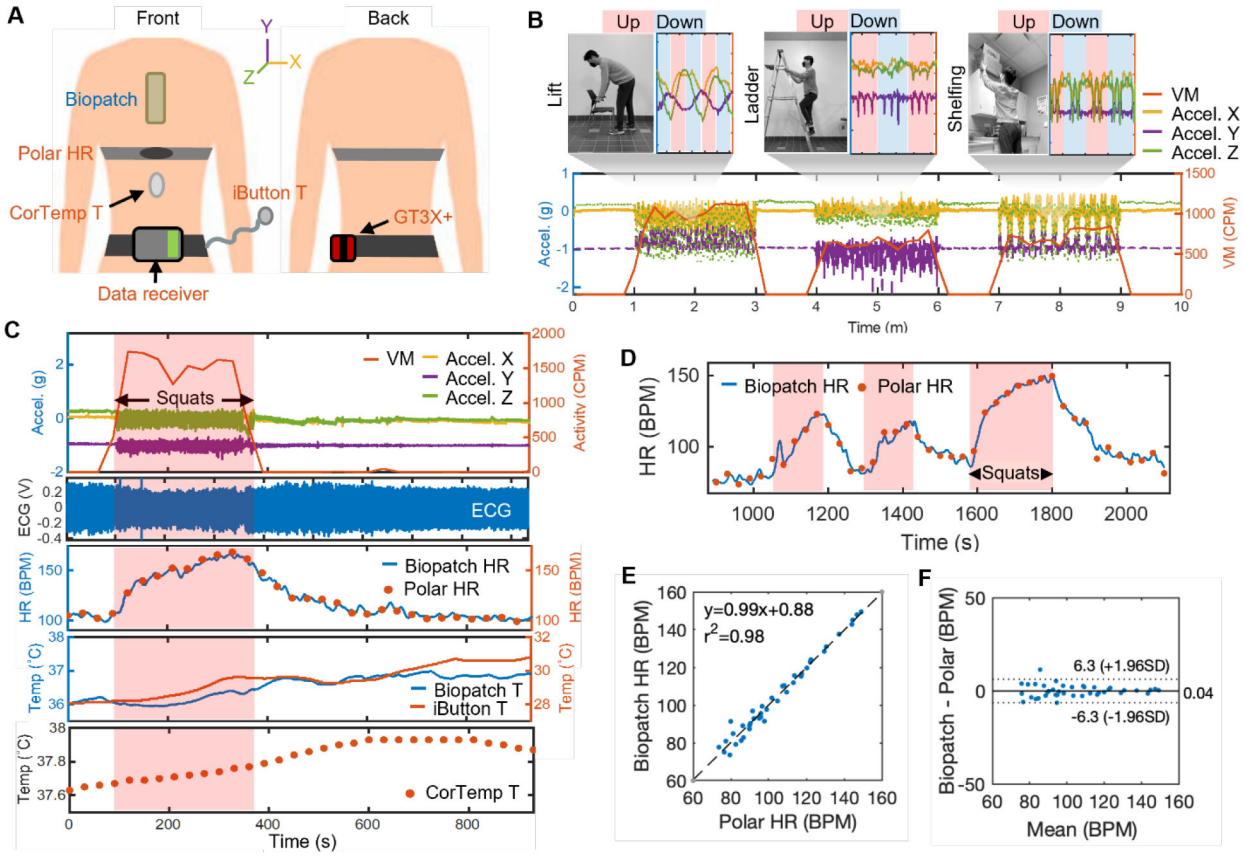

Figure 4. Evaluation of biopatch's sensing performance.

(A) Illustration of devices used in the comparison study and attachment locations for a biopatch and multiple commercial devices. (B) Motion data captured by the biopatch and GT3X+ during simulated tasks, including lifting, ladder climbing, and shelfing. (C) Full data captured by the biopatch and commercial devices during an outdoor exercise protocol. (D) Two HR data from the biopatch's ECG and Polar HR chest strap, overlaid to visualize the level of agreement during an outdoor exercise protocol. (E) Correlation analysis showing a highly linear relationship with the correlation coefficient of two devices. (F) Comparison of mean bias data between the two sets of HR data. Dashed lines indicate ± 1.96 SD while the center solid line represents the mean bias of +0.04 BPM.

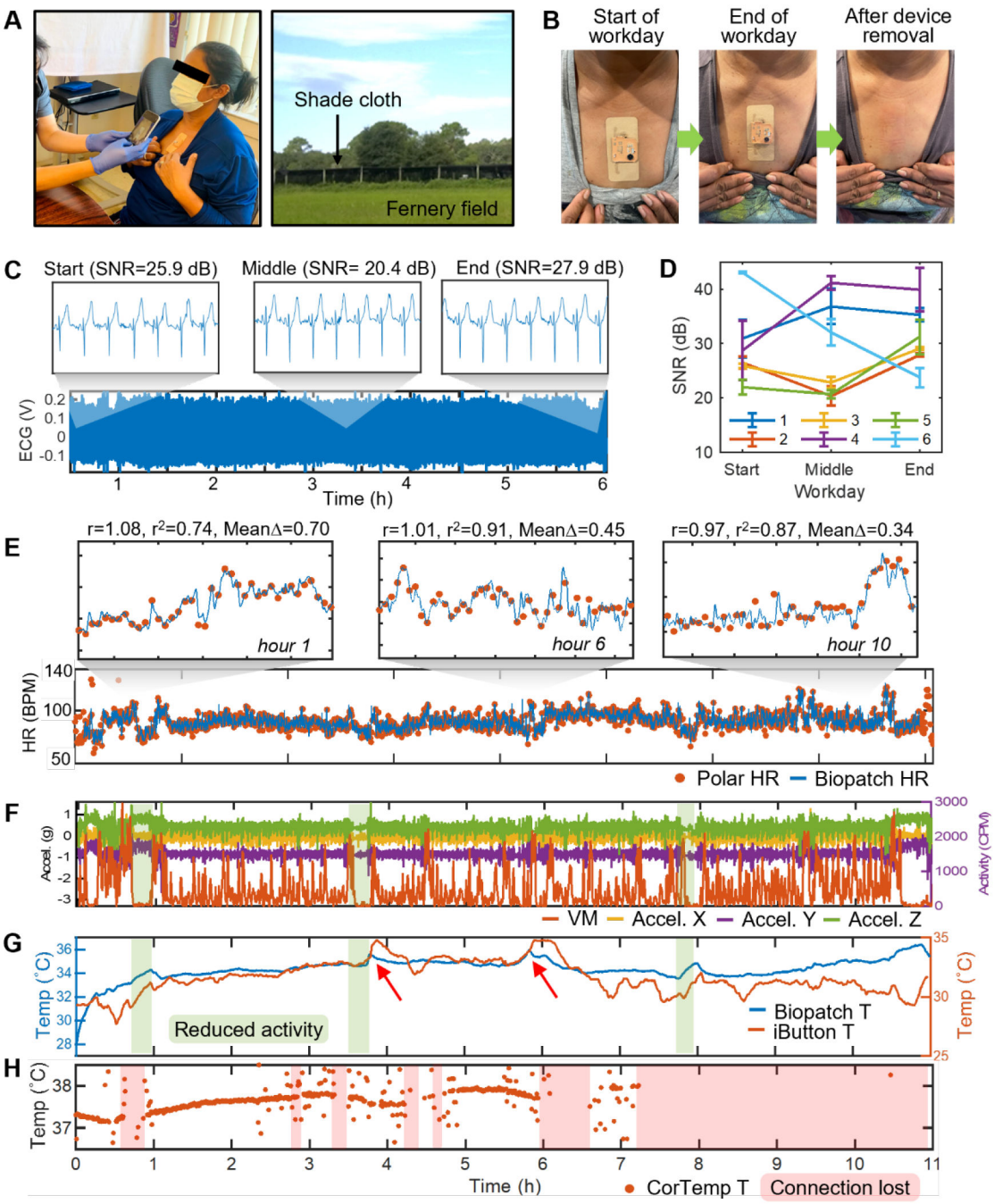

Figure 5. Deploying biopatch for health monitoring of agricultural workers.

(A) Application of the biopatch to a farmworker at the beginning of a workday (left). Photograph of a typical fernery field at the study site (right). (B) Photographs showing the device conditions at the beginning and end of a workday as well as the skin conditions immediately after the biopatch removal. (C) 6 hour-long ECG data from Participant #2 with zoomed sections showing the details of the waveform and respective SNR values at the start, middle, and end of the workday. (D) SNR of ECG at the start, middle, and end of all workdays for the six participants. Data are mean ± SD (n = 5). (E) Comparison of

HR data measured from Participant #1 over the eleven hour-long workdays. 20 min-wide zoomed sections in hours 1, 6, and 10 show consistently high linear correlation and agreement between the two data. (F) Activity data recorded by GT3X+ and the biopatch. Sections colored in green represent time windows of reduced activity. (G) Skin and ambient temperature recorded by the biopatch and iButton, respectively. Red arrows point to the biopatch's temperature sensor responding to large increases in the ambient temperature. (H) T_c recorded by CorTemp's ingestible pill sensor. Sections colored in red indicate lost wireless connectivity between the pill sensor and the waist-worn receiver unit.

Table 1.

Comparison of recent studies on health monitoring of workers with wearable devices.

Ref.	Target users	Form factor	Continuous monitoring w/o data loss	High-temperature operation	Sweat management	Field validation	Measured modalities	Connectivity/ Data management
This work	*Farm workers*	*All-in-one, soft patch*	*Yes*	*Yes*	*Yes*	*Yes*	*ECG, HR, Temperature, Activity*	*Wireless/Real-time data display, Offline analysis*
Shakerian et al. (2021)	Construction workers	Wristband	No (device movement)	No	No	No	EDA, Temperature, PPG	Wireless/ Offline analysis
Baghdadi et al. (2021)	Worker fatigue	Rigid box, strap	No	No	No	No	Activity	Wireless/ Offline analysis
Lu et al. (2020)	Driver fatigue	Thin sensor prototype, wires	No (wire movement)	No	No	No	Facial motion	Wired/Offline analysis
Allik et al. (2019)	Physical workers	Rigid box, strap	No (device movement)	No	No	No	ECG, HR, HRV	Wireless/ Offline analysis
Mac et al. (2017)	Farm workers	Rigid box, belt, strap	No (device movement, wireless interference)	No	No	Yes	HR, Core body temperature, Ambient temperature, Activity	Wireless/ Offline analysis
Aryal et al. (2017)	Construction workers	Rigid box, strap, headset, wristband	No (device movement)	No	No	No	HR, Temperature, EEG	Wireless/ Offline analysis
Shortz et al. (2017)	Oil extraction workers	Rigid box, strap	No (wires, device movement)	No	No	No	HRV	Wireless/ Offline analysis
Morales et al. (2017)	Drivers	Headset	No (device movement)	No	No	No	EEG, Eye motion	Wireless/ Offline analysis
Lee et al. (2017)	Construction workers	Rigid box, strap, wristband	No (device movement)	No	No	Yes	ECG, HR, Activity	Wireless/ Offline analysis
Gatti et al. (2014)	Construction workers	Rigid box, belt, strap	No (Device movement)	No	No	No	HR, RR	Wireless/ Offline analysis